Measurements of Bubbly Flow on a 4x4 Rod Bundle Under Oscillating Conditions

Tan Hung Hoang[1], Myung Ho Kim[2], Byoung Jea Kim[1]
School of Mechanical Engineering, Chungnam National University, Daejeon, Republic of Korea
System Engineering dept., ITER Korea Institute of Fusion Energy, Daejeon, Republic of Korea
bjkim@cnu.ac.kr

***Keywords:** rod bundle, local bubble parameters, rolling condition, optical-fiber Doppler probe

1. Introduction

The attraction of the Floating Nuclear Power Plant (FNPP) has increased worldwide because this is a reliable supply of energy far out to sea, on an island, or in a coastal community and is a part of the solution for climate change and the transition to Net Zero [1]. Depending on the ocean condition, the thermal-hydraulic behavior and safety characteristics of the FNPP may differ from those of conventional nuclear power plants. The main types of floating platform motions include heaving, rolling, pitching, yawing, swaying, and surging [2]. The analysis shows that the rolling motion and pitching motion are the most complex [3]. The bubble behavior is essential for flow boiling and nuclear safety. Some experiments under the rolling motion were conducted in vertical rectangular channels and rod bundles. However, the measurements of the local bubble parameters in rod bundles under rolling conditions are limited. In this study, the experiment was performed to measure the local bubble parameters in the rod bundle under rolling conditions. An optical-fiber Doppler probe was used to measure the void fraction, bubble velocity, and bubble size. The data from the experiment can be used to validate the model of numerical analysis and develop the flow pattern picture of ocean motions.

2. Experiment works

2.1 Experiment facility

Fig. 1 shows the schematic diagram of the experimental setup and cross-section of the 4×4 rod bundle. The experimental setup consists of a circulating pump, electromagnetic flow meters, an air compressor, a mass flow controller (MFC), a water tank, and a rod bundle mounted on a rolling platform. The air supplied from the compressor was fed into the lower part of the test section through the MFC and a porous plate of 5 mm in thickness, 0.21 of porosity, and 5 microns of pores to generate small bubbles. Water supplied from the pump was introduced to the lower part and mixed with bubbles to make the bubbly flow. The test section made of transparent acrylic is a square channel with a width, depth, and height of 100.8, 100.8, and 900 mm, respectively. Sixteen rods with a diameter of 19 mm were installed in a 4x4 square lattice arrangement with 6.2 mm between two adjacent rods.

An optical-fiber Doppler probe (OFDP) was used to measure the local time-averaged bubble parameters in the cross-sectional plane at 800 mm from the inlet. The ratio of z/D = 48.3 to avoid the hydrodynamic entrance effect. The OFDP was mounted in a 2-stage transfer system driven by servo motors to enable precise positional adjustment (positioning accuracy 0.01 mm). By the symmetry of configuration, one-fourth of the center subchannel was selected to measure with a total of 61 points, as shown in Fig.2.

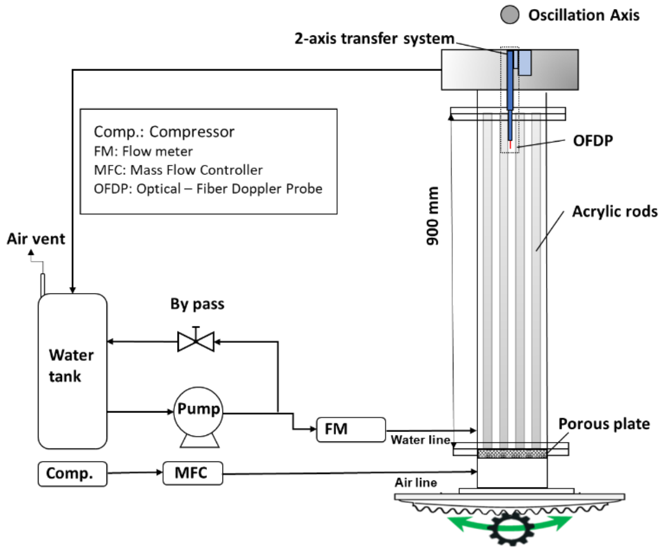

Fig.1 Schematic of the experiment setup

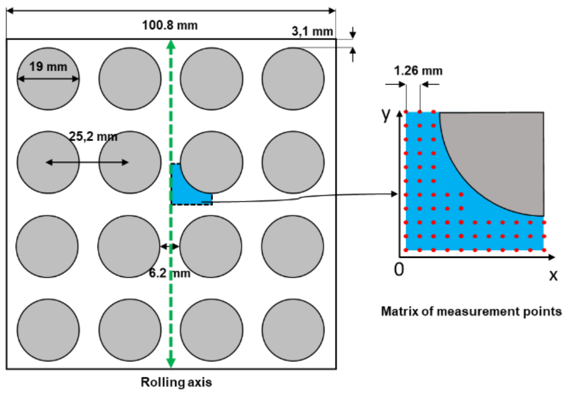

Fig.2 Cross-section and matrix of measurement points

The rolling axis was 1.2 m from the inlet, and the rolling motion of the platform can be expressed as follows:

$$\theta(t) = \theta_{max}\sin(2\pi t/T) \quad (1)$$

$$\Omega(t) = (2\pi/T)\theta_{max}\cos(2\pi t/T) \quad (2)$$

$$\phi(t) = -(4\pi^2/T^2\ \theta_{max}\cos(2\pi t/T) \quad (3)$$

where $\theta(t)$, $\Omega(t)$, $\phi(t)$, θ_{max}, and T denote the rolling amplitude, rolling angular velocity, rolling angular acceleration, maximum rolling amplitude, and rolling period, respectively. Fig.3 presents the oscillation characteristics of $\theta_{max} = 10°,\ T = 10s$.

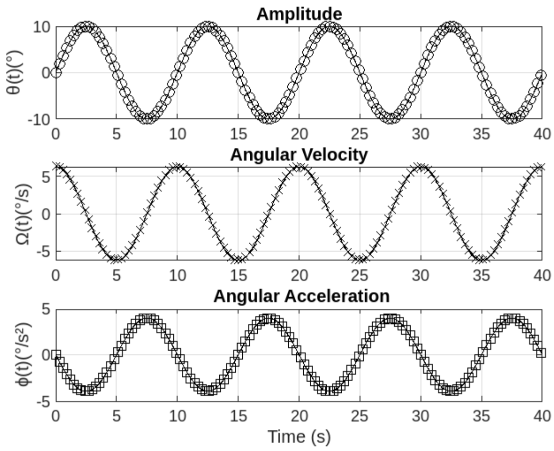

Fig.3 Rolling motion characteristics of $\theta_{max} = 10°, T = 10s$

2.2 Measurement method

Local void fraction, bubble diameter, and bubble velocity were measured by a single OFDP as shown in Fig.4. A laser is emitted inside the probe and gets reflected at the probe tip; based on the reflected light intensity, the phases can be distinguished. In this case, when the probe tip is surrounded by water, the output signal remains at a low level and vice versa when the probe tip is surrounded by a bubble. The void fraction is computed as the sum of all gas durations divided by the total experiment duration. To measure size/velocity of bubble, the Doppler effect is used. When the bubble gets close enough to the probe tip, the bubble interface reflects the laser light emitted from the optical probe and creates an interference phenomenon. By analyzing the frequency, the bubble velocity is determined. The diameter of bubble can be obtained from the velocity above and the residence time of the probe tip inside the bubble. At each measurement location, data were acquired for 180 seconds for void fraction and 500 samples for bubble size and velocity. The maximum errors of the bubble parameters were approximately 10% in this study.

2.3 Experiment conditions

The experiment was conducted with two conditions of inlet flow rate with the average superficial air velocity,$\langle j_g \rangle$,set at 0.024 m/s and the average superficial water velocities, $\langle j_l \rangle$, set at 0.192 and 0.058 m/s as shown in Table 1. With each flow condition, vertical standing and rolling oscillation with two rolling amplitudes (θ_{max} = 5°, 10°), and two rolling periods (T = 6, 10 s) were considered.

Table 1. Inlet flow conditions

	$\langle j_g \rangle$ (m/s)	$\langle j_l \rangle$ (m/s)
Case 1	0.024	0.192
Case 2	0.024	0.058

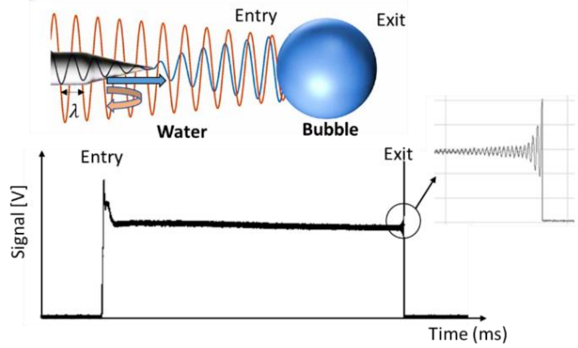

Fig.4 Bubble velocity/size measuring process of the OFDP.

3. Results and discussions

The local time-averaged void fraction distribution of Case 1 and Case 2 under the stationary state is shown in Fig.5. Based on the results, the void fraction distribution in Case 1 exhibits a local maximum between the two rods, whereas in Case 2, as the average void fraction increases, the peak shifts to the center of the subchannel as the water velocity decreases.

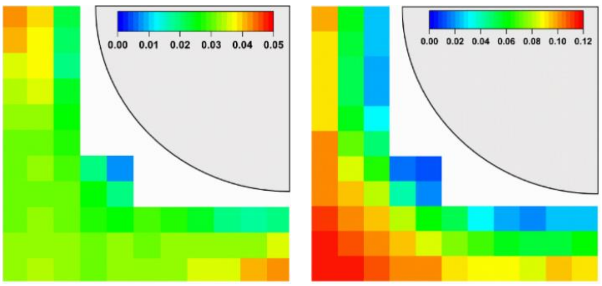

(a) (b)

Fig.5 Void fraction distribution at vertical standing condition: (a) Case 1; (b) Case 2.

Fig.6 and Fig.7 show the local time-averaged void fraction distribution at the center channel in different rolling amplitudes and periods. The void fraction distribution shows a general trend of increasing in the direction perpendicular to the rolling axis while decreasing in the direction along the rolling axis. In case 1, the rolling period has a significant effect on the void fraction distribution. At the same rolling amplitude, a change of rolling period from 6 to 10 seconds shows clearly increasing of void in the direction perpendicular to the rolling axis.

Fig.7 shows the time-averaged void fraction distribution of Case 2 under various rolling conditions. Under a rolling amplitude of 5 degrees, the peak of the void fraction is at the center of the subchannel. Similar results were shown in the stationary state for both rolling periods. The distribution of the void fraction became flatter when the rolling amplitude increased to 10 degrees. It can be seen that the effect of rolling amplitude on void fraction, the void fraction significantly decreases in the center region when the rolling amplitude increases, because the bubbles from the center channel move to the adjacent channel due to dynamic changes in gravity.

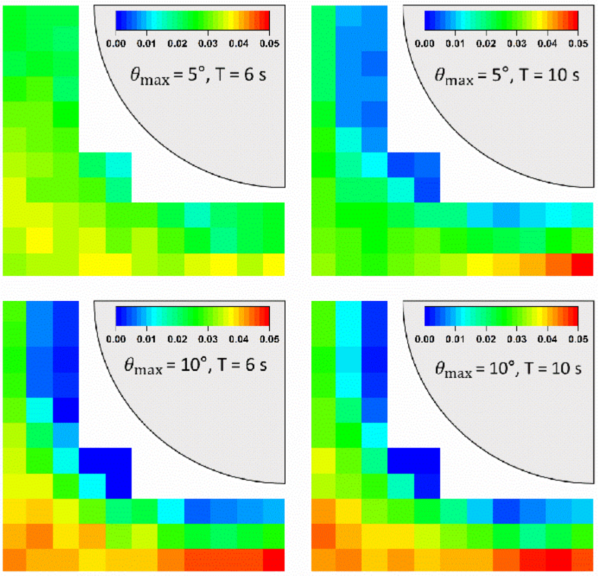

Fig.6 Void fraction distribution under rolling conditions of Case 1

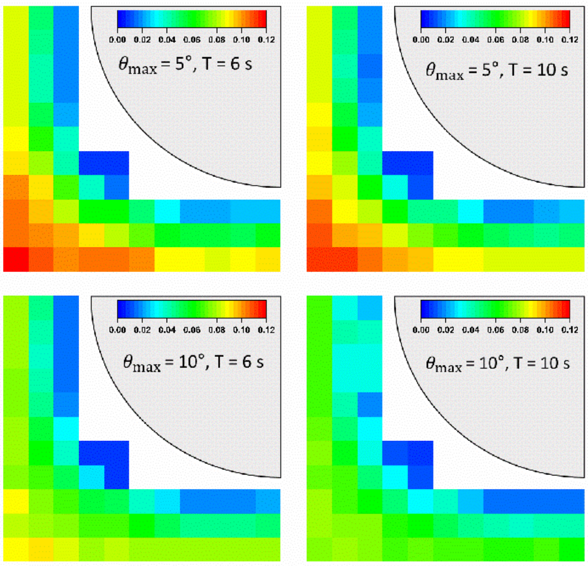

Fig.7 Void fraction distribution under rolling conditions of Case 2

4. Conclusions

Measurement of local bubble parameters in the center subchannel of the 4x4 rod bundle under oscillating conditions was conducted by using an optical-fiber Doppler probe. Bubbly flow with a local peak of void fraction depends on inlet flow conditions. In general, under rolling conditions, bubbles tended to concentrate along to rolling axis. Depending on the initial void distribution, both rolling amplitude and period have differential influence levels. Future work will focus on numerical analysis was validated against experimental data under stationary conditions and rolling conditions.

5. Acknowledgements

This work was supported by grants from the National Research Foundation of Korea, funded by the Ministry of Science and ICT (No. 2021M2D2A1A02039565).

6. References

[1] IAEA, "Advances in small modular reactor technology developments," Austria, 2022.

[2] I. ISHIDA, T. KUSUNOKI, H. MURATA, T. YOKOMURA, M. KOBAYASHI, and H. NARIAI, "Thermal-hydraulic behavior of a marine reactor during oscillations," *Nuclear Engineering and Design* vol. 120, pp. 213-225, 1990.

[3] B. H. Yan, "Review of the nuclear reactor thermal hydraulic research in ocean motions," *Nuclear Engineering and Design*, vol. 313, pp. 370-385, 2017, doi: 10.1016/j.nucengdes.2016.12.041.